Lopez-Morales, M. J., Chen-Hu, K. & Garcia-Armada, A. (2022) 2021). *Effect of Spatial Correlation on the Performance of Non-coherent Massive MIMO based on DMPSK, In: 2021 IEEE Global Communications Conference (GLOBECOM), Madrid, Spain,* 7-11 Dec. 2021, 6 p.

DOI: https://doi.org/10.1109/GLOBECOM46510.2021.9685812

Effect of Spatial Correlation on the Performance of Non-coherent Massive MIMO based on DMPSK

Manuel Jose Lopez Morales
Universidad Carlos III de Madrid
Madrid, Spain
mjlopez@tsc.uc3m.es

Kun Chen-Hu
Universidad Carlos III de Madrid
Madrid, Spain
kchen@tsc.uc3m.es

Ana Garcia Armada
Universidad Carlos III de Madrid
Madrid, Spain
agarcia@tsc.uc3m.es

***Abstract*—A rigorous analysis of the effect of spatial correlation for non-coherent (NC) massive multiple-input-multiple-output (MIMO) in Rician channels is important to determine its applicability in these scenarios. We conduct such analysis for a single base station (BS) and a more general case of several BSs, all of them showing correlation among their own antennas but with uncorrelated channels with respect to each other. We first perform an analysis of the distribution of the received symbols, then propose some approximations to give a closed form expression of the symbol error probability (SER) and the signal-to-interference-and-noise-ratio (SINR) as performance measures. Finally, we extract some conclusions from this analysis to show how the combined use of several BSs and larger Rician components can be beneficial in this scenario. Some numerical results are added to confirm the accuracy of the analysis.**

***Index Terms*—Non-coherent, massive MIMO, differential modulation, spatial correlation, C-RAN.**

I. Introduction

MASSIVE multiple-input-multiple-output (MIMO) is a technology where a base station (BS) is equipped with several antennas [1]. In these systems, the channel is estimated and compensated to perform coherent detection. Several reference signals (pilots) must be used to estimate the channel state information (CSI). In high mobility, high frequency selectivity and/or low SNR scenarios, the use of CSI is problematic, since many pilots may be needed [2], [3], thus making the coherent processing potentially unfeasible.

Non-coherent (NC) massive MIMO allows to receive data without using CSI while benefiting from using many antennas at the BS and also reducing the complexity of the receivers. Reference [2] showed that NC detection can perform well in extremely time-varying channel scenarios, while the coherent scheme fails. A widely used NC technique is based on differential M-ary phase shift keying (DMPSK) [4], combined with differential detection. The NC performance superiority in complicated scenarios makes it a good option in future communication systems [2], [3].

Furthermore, BS antenna arrays suffer from spatial correlation caused by the antenna elements coupling, the array geometry and the propagation channel [5], [6], which reduces the spatial diversity in the receiver. For the NC massive MIMO, most of the literature considers uncorrelated channels [4], [7], while [8] made use of a geometric wide-band channel model, but did not perform a rigorous theoretical analysis of the effects of spatial correlation. Such analysis has not been done in the literature to the best knowledge of the authors.

The contribution of this paper is a mathematical analysis of the effect of the spatial correlation for a single-user NC massive MIMO system based on DMPSK. We consider Rician channels and derive the SER and the SINR for a single BS and for several BSs that may cooperate, for the same number of total antennas. Since the BSs are distant from each other, their channels will not be correlated, even though locally experiencing spatial correlation among the antennas of each of them. Thus, it is expected that the multi-BS scenario performs better. We also show that the NC massive MIMO can benefit from the presence of a strong Rician component. Furthermore, we show that NC massive MIMO can improve its performance when a coordinated detection is done over several BSs. These same effects happen for coherent massive MIMO, which reinforces the validity of NC schemes. Since practical implementations of massive MIMO have low hundreds antennas for the largest commercial arrays, a coordinated detection over several BSs is of interest to have a larger spatial diversity. This model is typical, for instance, in classical coherent ultra-dense networks (UDN) based on cloud-RAN and cell-free massive MIMO [9], [10]. These systems may suffer from high computational complexity and a large training overhead for CSI estimation. Thus, a non-coherent approach can take advantage of the uncorrelated channel among BSs and can overcome the limitations of UDN deployments, while making them feasible in scenarios of high mobility, high frequency selectivity and low SNR [2], [3].

The remainder of this paper is organized as follows. We first introduce the system model in Sec. II. We derive the statistical distribution of the received symbol in a Rician spatially correlated channel for non-coherent massive MIMO, we compute the expressions of the SER and SINR and we extract some remarks from the analysis of the distribution and the expressions in Sec. III. Some numerical results in Sec. IV confirm our theoretical derivations. Some conclusions and future work are pointed out in Sec. V.

Notation: matrices, vectors and scalar quantities are denoted

This work has received funding from the European Union Horizon 2020 research and innovation programme under the Marie Skłodowska-Curie ETN TeamUp5G, grant agreement No. 813391, and the Spanish National Project TERESA-ADA (TEC2017-90093-C3-2-R) (MINECO/AEI/FEDER, UE).

by boldface uppercase, boldface lowercase, and normal letters, respectively. $[\mathbf{A}]_{m,n}$ denotes the element in the m-th row and n-th column of $\mathbf{A}$. $[\mathbf{a}]_n$ represents the n-th element of vector $\mathbf{a}$. The superscripts $(\cdot)^H$, $(\cdot)^*$ and $*$ denote Hermitian complex conjugate and convolution, respectively. $\mathbb{E}\{\cdot\}$ represents the expected value. $\mathcal{CN}(0,\sigma^2)$ represents the circularly-symmetric and zero-mean complex normal distribution with variance σ^2. $\Re\{(\cdot)\}$ and $\Im\{(\cdot)\}$ refer, respectively, to the real and imaginary parts of a complex number. $||x||_2$ denotes the euclidean norm of x. $\mathbf{1}$ and $\mathbf{0}$ indicate a column vector of all ones and all zeros, respectively. $Q(\cdot)$ indicates the Q-function.

II. System model

We consider a generic massive MIMO system with A BSs, with R_a antennas in BS a, and we focus on a particular single-user with one antenna. When $A = 1$ we have a classical massive MIMO with non-cooperative BSs and for $A > 1$ we have the case of network MIMO, cell-free massive MIMO and related works [9]–[11]. In case of cooperation, it is assumed that the BSs are connected to a central processing unit (CPU) by means of a fronthaul. In this paper, we do not take into account fronthaul constraints and suppose the fronthaul to be ideal. We focus on the particular case of uplink (UL), where the user transmits a differentially encoded signal in the following manner at time instant n

$$x_n = x_{n-1}s_n \quad 1 \le n \le N, \tag{1}$$

where s_n belongs to a DMPSK constellation and x_0 is a reference symbol known at the receiver side and necessary to perform the differential reception. Because the information is only encoded in the phase, we know that $x_n^* x_{n-1} = s_n$.

The propagation channel between the user and the BS a at time instant n is represented by $\mathbf{g}_{n,a}$ $(R_a \times 1)$. In detail,

$$\mathbf{g}_{n,a} = \bar{\mathbf{h}}_{n,a} + \hat{\mathbf{h}}_{n,a}, \tag{2}$$

where $\mathbf{g}_{n,a}$ $(R_a \times 1)$ represents small-scale fading $\mathbf{g}_{n,a} \sim \left(\bar{\mathbf{h}}_{n,a}, \sigma^2_{h,a}\mathbf{R}_{n,a}\right)$, $\bar{\mathbf{h}}_{n,a}$ is a vector of size $(R_a \times 1)$ that remains constant over several coherence intervals and where all elements are equal to $|\bar{h}_{n,a}|e^{j\theta_{n,a}}$, with

$$|\bar{h}_{n,a}|^2 = \frac{K_a}{K_a+1} \qquad \text{and} \qquad \sigma^2_{h,a} = \frac{1}{K_a+1}, \tag{3}$$

where K_a is the Rician factor, which characterizes the fading model. For $K_a = 0$, the model collapses to Rayleigh. $\mathbf{R}_{n,a}$ is a normalized Hermitian matrix of size $(R_a \times R_a)$. For correlated fading and to obtain a closed-form expression in Section III, we use a classical correlation model [12] found often in the literature for $\mathbf{R}_{n,a}$ as, with $|r-r'|$ the distance between antenna r and r'

$$\left[\mathbf{R}_{n,a}\right]_{r,r'} = \delta^{|r-r'|} \quad \text{with} \quad 0 \le \delta \le 1. \tag{4}$$

Using this model, we give some insights on the effects of the spatial correlation in Section III-C. For $\delta = 0$, the Hermitian matrix collapses to $\mathbf{R}_{n,a} = \mathbf{I}_{R_a}$ which represents uncorrelated fading. We assume that the channel in two consecutive time instants can be regarded as equal $\mathbf{g}_{n-1} = \mathbf{g}_n$, for any antenna. The channel coefficients between BSs are uncorrelated as

$$\mathbb{E}\left\{\mathbf{g}^H_{n,a}\mathbf{g}_{n,a'}\right\} = \mathbf{0} \quad \forall a \neq a' \tag{5}$$

and the received signal at BS a and n-th time instant is

$$\mathbf{y}_{n,a} = \mathbf{g}_{n,a}x_n + \boldsymbol{\nu}_{n,a}, \tag{6}$$

where x_n denotes the transmitted symbol at time n by the user of interest and $\boldsymbol{\nu}_{n,a}$ $(R_a \times 1)$ represents the additive white Gaussian noise according to $\boldsymbol{\nu}_{n,a} \sim \mathcal{CN}(\mathbf{0}, \sigma_a^2\mathbf{I}_{R_a})$. Finally, the signal-to-noise-ratio (SNR) in access point a is defined as $\rho_a = \sigma_a^{-2}$, where we set the power of the transmitted symbols to one and the SINR is referred as ρ.

In reception at each BS a, two contiguous differential symbols in the time domain are non-coherently combined as

$$z_{n,a} = \mathbf{y}^H_{n-1,a}\mathbf{y}_{n,a}. \tag{7}$$

In a scenario with $A > 1$ BSs (multi-BS), the variables z_a in each BS are sent to the CPU and combined as

$$z_n = \frac{\sum_{a=1}^{A} z_{n,a}}{\sum_{a=1}^{A} R_a}, \tag{8}$$

which is the variable over which the transmitted symbols are estimated according to [4] as

$$\hat{s}_n = \arg\min_{s_n} \left\{ |s_n - z_n|, \ s_n \in \mathfrak{M} \right\}, \tag{9}$$

where $\mathfrak{M}$ indicates the DMPSK constellation set.

III. Effect of the spatial correlation for non-coherent massive MIMO based on DMSPK

In this section we perform the analysis of the distribution of the received symbol z. With the knowledge of that distribution, we give closed-form expressions of the SER and the SINR for the received symbol z. Last, we provide some remarks about the distribution of the received symbol.

A. Distribution of the received symbol z

With some derivations, (7) can be expanded as

$$\begin{aligned} z_a = &\underbrace{\left(\mathbf{g}_{n-1,a}x_{n-1}\right)^H \mathbf{g}_{n,a}x_n}_{z_a^{(1)}} + \underbrace{\left(\boldsymbol{\nu}_{n-1,a}\right)^H \boldsymbol{\nu}_{n,a}}_{z_a^{(2)}} + \\ &+ \underbrace{\left(\boldsymbol{\nu}_{n-1,a}\right)^H \mathbf{g}_{n,a}x_n}_{z_a^{(3)}} + \underbrace{\left(\mathbf{g}_{n-1,a}x_{n-1}\right)^H \boldsymbol{\nu}_{n,a}}_{z_a^{(4)}} \end{aligned} \tag{10}$$

where (and since $\mathbf{g}_{n-1,a} = \mathbf{g}_{n,a}$, $\bar{\mathbf{h}}_{n,a} = \bar{\mathbf{h}}_{n-1,a}$ and $\hat{\mathbf{h}}_{n,a} = \hat{\mathbf{h}}_{n-1,a}$) each element expands as

$$\begin{aligned} z_a^{(1)} &= \left(\mathbf{g}_{n-1,a}x_{n-1}\right)^H \mathbf{g}_{n,a}x_n = \\ &= \left(\bar{\mathbf{h}}_{n-1,a} + \hat{\mathbf{h}}_{n-1,a}\right)^H \left(\bar{\mathbf{h}}_{n,a} + \hat{\mathbf{h}}_{n,a}\right) s_n = \\ &= \Big(\underbrace{\left\|\bar{\mathbf{h}}_{n,a}\right\|_2^2}_{z_a^{(1,1)}} + \underbrace{2\Re\{\bar{\mathbf{h}}^H_{n,a}\hat{\mathbf{h}}_{n,a}\}}_{z_a^{(1,2)}} + \underbrace{\left\|\hat{\mathbf{h}}_{n,a}\right\|_2^2}_{z_a^{(1,3)}} \Big) s_n, \end{aligned} \tag{11}$$

$$z_a^{(2)} = \boldsymbol{\nu}^H_{n-1,a}\boldsymbol{\nu}_{n,a}, \tag{12}$$

$$z_a^{(3)} = \boldsymbol{\nu}_{n-1,a}^H \mathbf{g}_n x_n = \underbrace{\boldsymbol{\nu}_{n-1,a}^H \bar{\mathbf{h}}_{n,a} x_n}_{z_a^{(3,1)}} + \underbrace{\boldsymbol{\nu}_{n-1}^H \hat{\mathbf{h}}_{n,a} x_n}_{z_a^{(3,2)}}, \quad (13)$$

$$z_a^{(4)} = (\mathbf{g}_{n-1} x_{n-1})^H \boldsymbol{\nu}_n = \underbrace{\bar{\mathbf{h}}_{n-1,a}^H \boldsymbol{\nu}_n x_{n-1}^*}_{z_a^{(4,1)}} + \underbrace{\hat{\mathbf{h}}_{n-1,a}^H \boldsymbol{\nu}_n x_{n-1}^*}_{z_a^{(4,2)}}. \quad (14)$$

Using the properties of the product of normal variables [13], and variance-gamma distributions [14], [15] for $\sum_a R_a \to \infty$, $z_a^{(2)}$, $z_a^{(3,1)}$, $z_a^{(4,1)}$, $z_a^{(3,2)}$ and $z_a^{(4,2)}$ are distributed as

$$z_a^{(2)} \sim \mathcal{CN}\left(0, R_a \sigma_{\nu,a}^4\right), \quad (15)$$

$$z_a^{(3,1)}, z_a^{(4,1)} \sim \mathcal{CN}\left(0, R_a |\bar{h}_a|^2 \sigma_{\nu,a}^2\right), \quad (16)$$

$$z_a^{(3,2)}, z_a^{(4,2)} \sim \mathcal{CN}\left(0, R_a \sigma_{h,a}^2 \sigma_{\nu,a}^2\right). \quad (17)$$

The term $z_a^{(1,1)}$ is the line-of-sight (LoS) component which is assumed to vary slowly with respect to the coherence time of the channel, so it can be regarded as deterministic in our statistical analysis. Taking into account that each element of $\hat{\mathbf{h}}$ is a zero-mean circularly symmetric Gaussian variable, the phase rotation produced by the phase of $\bar{\mathbf{h}}$ does not change its distribution so $\Re\{\bar{\mathbf{h}}^H \hat{\mathbf{h}}\} = |\bar{h}| \Re\{\mathbf{1}^T \hat{\mathbf{h}}\}$. Following [16], the mean of the sum of normal variables scaled by any constant is the sum of all the means scaled by that constant. The variance is the sum of all the elements in the covariance matrix, scaled by the square of the constant. Also, since the real operation keeps half of the total variance when the distribution is circularly symmetric complex Gaussian, then

$$z_a^{(1,2)} \sim \mathcal{N}\left(0, 2|\bar{h}_a|^2 \sigma_{h,a}^2 \mathbf{1}^T \mathbf{R}_{n,a} \mathbf{1}\right), \quad (18)$$

where $\mathbf{1}^T \mathbf{R}_{n,a} \mathbf{1}$ is strictly positive and represents the sum of all the elements in the Hermitian matrix $\mathbf{R}_{n,a}$. Last, in $\left\|\hat{\mathbf{h}}\right\|_2^2$, each element follows a Gamma distribution, and the elements are correlated among them, with a covariance matrix following [17], so according to the properties of Gamma distributions [18], $z_a^{(1,3)}$ is distributed as

$$z_a^{(1,3)} \sim \mathcal{N}\left(R_a \sigma_{h,a}^2, \sigma_{h,a}^4 \left\|\mathbf{R}_{n,a}\right\|_2^2\right). \quad (19)$$

B. Derivation of the SER and SINR

Due to the symmetry of DMPSK constellations, the SER and SINR of the constellation can be calculated using any symbol of the constellation. In this case we particularize for the symbol $s = 1$, without loss of generality. To compute the probability density function (PDF) of the decision variable z in (8), we have to take into account that it is the summation of A independent Gaussian distributed random variables. Applying straightforward manipulations and properties, the distribution of the real and imaginary parts of z for $s = 1$ is

$$\Re\{z\} \sim \mathcal{N}\left(\mu_\Re, \sigma_\Re^2\right) = \mathcal{N}\left(1, \frac{\sum_{a=1}^A \sigma_{\Re\{z_a\}}^2}{\left(\sum_{a=1}^A R_a\right)^2}\right) \quad (20)$$

$$\begin{aligned} 2\sigma_{\Re\{z_a\}}^2 = {} & 2\sigma_{h,a}^2 \left(\sigma_{h,a}^2 \left\|\mathbf{R}_{n,a}\right\|_2^2 + 2|\bar{h}_a|^2 \mathbf{1}^T \mathbf{R}_{n,a} \mathbf{1}\right) + \\ & + R_a \left(\sigma_{\nu,a}^4 + 2\sigma_{\nu,a}^2\right), \end{aligned} \quad (21)$$

and

$$\Im\{z\} \sim \mathcal{N}\left(\mu_\Im, \sigma_\Im^2\right) = \mathcal{N}\left(0, \frac{\sum_{a=1}^A R_a (\sigma_{\nu,a}^4 + 2\sigma_{\nu,a}^2)}{2\left(\sum_{a=1}^A R_a\right)^2}\right). \quad (22)$$

The SER can be approximated by following the approach in Appendix A of [2] as

$$P_s \approx 1 - \frac{\int_{-\pi/M}^{\pi/M} \int_0^\infty e^{-\left(\frac{r\cos(\gamma) - \mu_\Re}{\sqrt{2}\sigma_\Re}\right)^2} e^{-\left(\frac{r\sin(\gamma) - \mu_\Im}{\sqrt{2}\sigma_\Im}\right)^2} r dr d\gamma}{2\pi\sigma_\Re^2 \sigma_\Im^2}. \quad (23)$$

A closed-form expression of (23) is mathematically intractable, although the integral can be solved numerically. The SINR can be calculated as the inverse of the sum of the variances of the real and imaginary parts as shown in (24). It can be seen that the numerator of the SINR grows with the square of the sum of the total amount of antennas while the denominator grows with the sum of the square of the antennas in each BS. Then, the numerator grows faster than the denominator when several BSs are used, showing that multi-BS processing benefits the NC scheme.

Eq. (23) can be further approximated to a closed-form expression that does not require a numerical evaluation by assuming a circularly symmetric complex Gaussian distribution and using the expression for PSK error of [19] as

$$P_s \approx 2Q\left(\sqrt{2\rho} \sin\left(\frac{\pi}{M}\right)\right). \quad (26)$$

C. Remarks about the effects of spatial correlation

It is worth noting that the previous expressions can be particularized for different scenarios. For instance, for $A = 1$ and uncorrelated Rayleigh fading $\left(\bar{\mathbf{h}}_a, \sigma_{h,a}^2 \mathbf{R}_{n,a}\right) = \left(\mathbf{0}_a, \mathbf{I}_{n,a}\right)$, we obtain the results of Appendix A of [2].

Following the model defined in (4), the terms $\left\|\mathbf{R}_{n,a}\right\|_2^2$ and $\mathbf{1}^T \mathbf{R}_{n,a} \mathbf{1}$ are simplified to

$$R_a(\delta = 0) \leq \left\|\mathbf{R}_{n,a}\right\|_2^2 = R_a \frac{1 - \delta^{2R_a}}{1 - \delta^2} \leq R_a^2(\delta = 1), \quad (27)$$

$$R_a(\delta = 0) \leq \mathbf{1}^T \mathbf{R}_{n,a} \mathbf{1} = R_a \frac{1 - \delta^{R_a}}{1 - \delta} \leq R_a^2(\delta = 1). \quad (28)$$

If correlation increases, both (27) and (28) increase, thus increasing $\sigma_\Re^2$, which is the variance of (20). Therefore, the SER increases and the SINR decreases, degrading the performance of the system. Eq. (25) shows the SINR for the extreme cases of $\delta = 0$ and $\delta = 1$. It can be observed an R_a term in the second summand in the case $\delta = 1$ that multiplies the variance of the real part, while for $\delta = 0$ that term is not present. Besides that, in both cases, it can be observed that the second summand of the denominator tends to 0 with increasing K, so a strong Rician component benefits the performance. Interestingly, these conclusions are similar to those obtained for coherent cell-free schemes in [20].

$$\rho = \frac{\left(\sum_{a=1}^{A} R_a\right)^2}{\sum_{a=1}^{A}\left(R_a(\sigma_{\nu,a}^4 + 2\sigma_{\nu,a}^2) + \sigma_{h,a}^2(\sigma_{h,a}^2\left\|\mathbf{R}_{n,a}\right\|_2^2 + 2|\bar{h}_a|^2\mathbf{1}^T\mathbf{R}_{n,a}\mathbf{1})\right)} \tag{24}$$

$$\underset{\delta=0}{\rho} = \frac{\left(\sum_{a=1}^{A} R_a\right)^2}{\sum_{a=1}^{A} R_a\left(\sigma_{\nu,a}^4 + 2\sigma_{\nu,a}^2 + \sigma_{h,a}^2(1+|\bar{h}_a|^2)\right)} \quad \underset{\delta=1}{\rho} = \frac{\left(\sum_{a=1}^{A} R_a\right)^2}{\sum_{a=1}^{A} R_a\left(\sigma_{\nu,a}^4 + 2\sigma_{\nu,a}^2 + R_a\sigma_{h,a}^2(1+|\bar{h}_a|^2)\right)} \tag{25}$$

Last but not least, it can be observed that the performance improves with the square of the sum of the number of antennas in each BS while it worsens with the sum of the square of the number of antennas in each BS (for the worst case of $\delta = 1$), so the performance always improves more when several BSs are used instead of just one.

IV. Numerical Results

In this section, we aim at checking that our analysis is correct and getting some insights on the effect of spatial correlation on the performance of NC massive MIMO. We show both the theoretical and the Monte-Carlo (obtained via simulations) results of the SER and SINR for the correlation model defined in (4). Different scenarios are simulated, with $A = 1$ and $R_a = 100$, $A = 10$ and $R_a = 10$, $A = 10$ and $R_a = 5$, $A = 1$ and $R_a = 50$, $A = 1$ and $R_a = 1000$ and $A = 1000$ and $R_a = 1$. The values of ρ_a, K_a and δ_a belong to a range depending on the shown results.

We have first performed a Kolmogorov-Smirnov (KS) test to check if both the theoretical and the Monte-Carlo distributions obtained for z can be regarded as the same. When $\delta < 0.9$, values that can be regarded as representative of realistic channels, the theoretical and Monte-Carlo distributions were regarded as the same for a standard significance value of 5%, confirming our analysis. On the contrary, for $\delta > 0.9$, the test for the real part of the distribution fails, which indicates that the distributions cannot be regarded as the same. Nevertheless, the goal is to check whether the analysis is valid for the SER and the SINR and to check if there is a discrepancy between the theoretical and Monte-Carlo results. Figs. 1 and 2 show that even though the discrepancy between the SER and SINR obtained by simulations and with the analysis in Section III is greater for high values of δ, the approximations still provide accurate results for those extreme values. The small discrepancy is due to the fact that the approximation of Gamma to Gaussian distributions is less valid with greater spatial correlation.

Fig. 1 shows the SER for SNR=0dB, against δ from 0.85 to 1. Both simulations and theoretical values are shown. We can observe how the SER increases with δ, which comes from the fact that the channel hardening is reduced. For the scenario with 10 BSs and 10 antennas per BS, the effect of δ is lower, which makes sense since the channels between BSs are uncorrelated. In Fig. 2, we can observe the SINR from the analysis and the simulated SINR for different SNR values, for $K = 0$, with two scenarios, one with $A = 1$ and $R = 100$ and one with $A = 10$ and $R = 10$. It can be observed that the analytical and the simulated SINR are very close to each other, confirming again the validity of the theoretical analysis, even for delta values approaching 1.

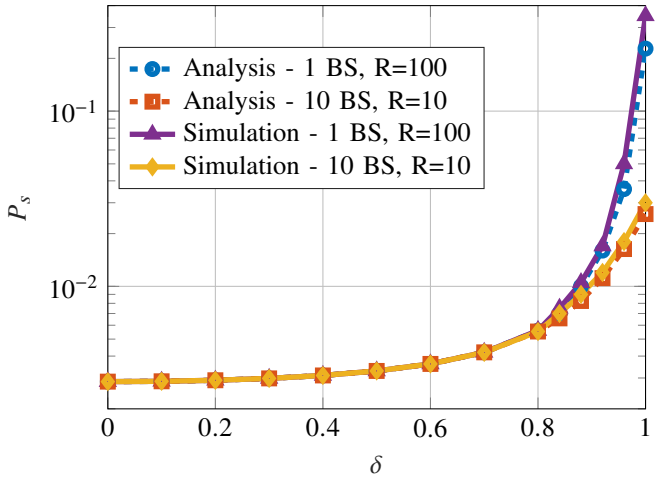

Fig. 1. SER vs δ for $M = 8$, $K = 0$ and $\rho_a = 0$dB.

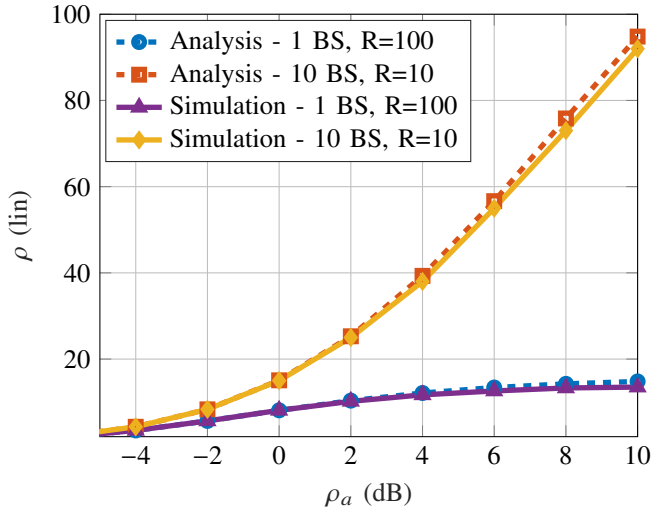

Fig. 2. SINR vs SNR for $M = 8$, $K = 0$ and $\delta = 0.99$.

In Fig. 3, we can see the SER versus the SNR for $\delta = 0$, $\delta = 0.7$, $\delta = 0.9$ and $\delta = 0.99$. We can see, again, that the greater the δ the greater the SER, but the effect is lower in the multi-BS scenario, which confirms the interest in the use of a coordinated massive MIMO network also for the NC

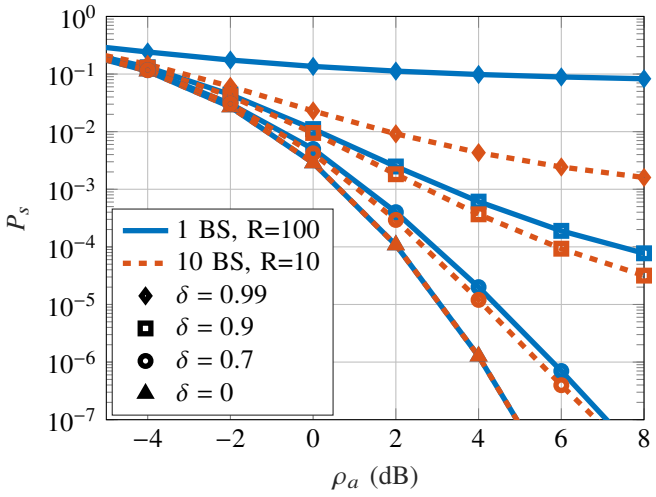

Fig. 3. SER vs SNR for $M = 8$ and $K = 0$, for different δ.

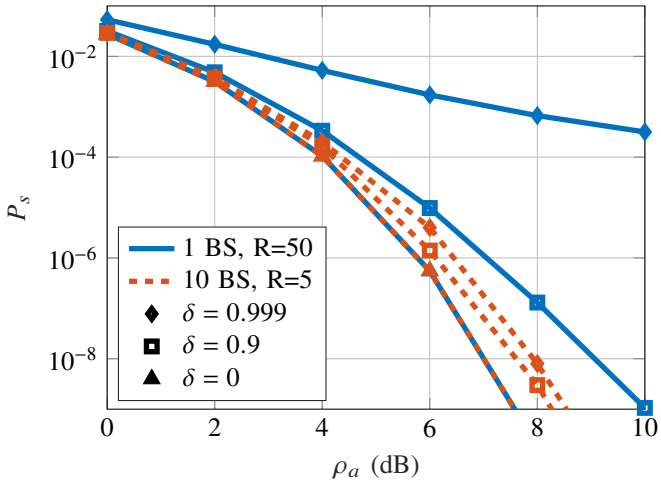

Fig. 4. SER vs SNR for $M = 8$ and $K = 30$, for different δ.

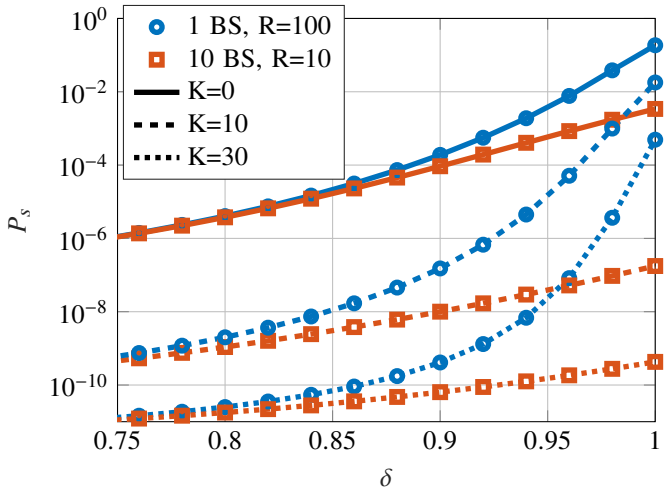

Fig. 5. SER vs δ for $M = 8$ and SNR=10dB for different K.

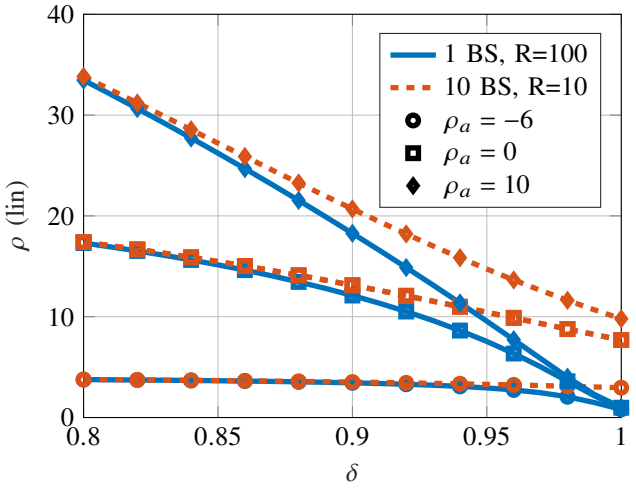

Fig. 6. SINR vs δ for $M = 8$ and $K = 0$, for different SNR.

DMPSK. Furthermore, if we consider a channel with a high deterministic component (Rician with strong LoS component), the non-coherent processing greatly benefits from the multi-BS scenario, as also shown in Fig. 4. In, fact the reduction in performance is almost negligible for $K = 30$ for high values of δ with respect to $\delta = 0$ in the case of A=10.

Fig. 5 shows the SER for different values of K for SNR=10dB. It can be seen how a high channel correlation (big δ values) greatly reduces (up to 9 orders of magnitude for $K = 30$) the performance for the scenario with 1 BS with respect to lower channel correlation (lower δ values). For the scenario with 10 BSs, that reduction in performance is lower (up to 4 orders of magnitude for $K = 0$), showing that the scenario with coordinated BSs is more resilient against a higher channel correlation than the scenario with a single BS. Besides this, a great improvement can be observed for the channels with a very strong deterministic component (high values of K). Fig. 6 and Fig. 7 show the SINR for different SNR and δ values. We can see that the multi-BS scenario has a lower reduction in SINR with respect to the single-BS scenario, which agrees with the results obtained for the SER.

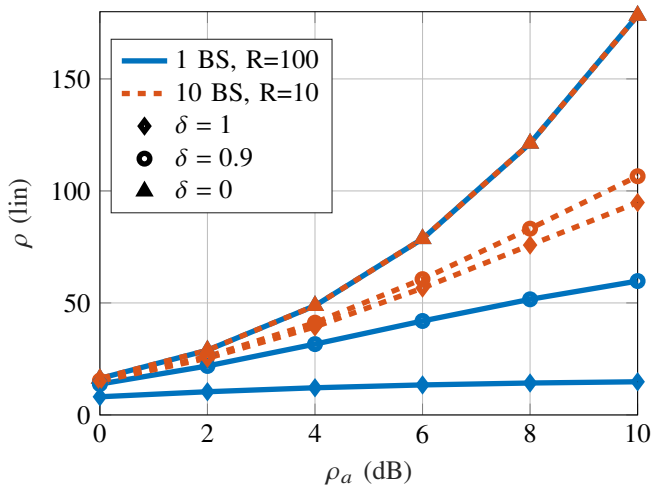

Fig. 7. SINR vs SNR for $M = 8$ and $K = 0$, for different δ.

Fig. 8 shows the SINR in dB for $\delta = 0.9$ for two cases, one

with $A = 1$ and $R_a = 100$ and one with $A = 100$ and $R_a = 1$. For low SNR, there is no increment in performance since the noise is the limiting factor. For $K = 0$, $K = 6$ and $K = 30$, an improvement can be observed for medium and high SNR of around 7.2dB, 9.8dB and 10dB, respectively. The improvement is greater for larger K.

For a better understanding of the relationship of the theoretical model with a realistic model, we simulated a geometric wide-band channel whose angular spread of the clusters is 25 degrees as the one simulated in [8]. The aim was to obtain the numerical results for $\left\|\mathbf{R}_{n,a}\right\|_2^2$ and $\mathbf{1}^T\mathbf{R}_{n,a}\mathbf{1}$, which are very similar to those obtained for the theoretical model particularized for $\delta = 0.9$. Therefore, lower angular spreads, which are realistic for certain scenarios, would result in greater δ values. Furthermore, no antenna correlation caused by antenna coupling was considered, which would be equivalent to greater values of δ. Nevertheless, we have shown that a non-coherent coordinated processing would be beneficial from $\delta = 0.5$, which then indicates that a benefit can be obtained for more general cases.

V. Conclusions

In this paper, we performed a theoretical analysis of the effect of Rician channels with correlation on the performance of single user uplink NC massive MIMO systems. We demonstrated that the greater the LOS component of the Rice channel, the better the performance. On the contrary, the greater the correlation between channels, the worse the performance. We showed how this detriment in performance is lower when several uncorrelated BSs with fewer antennas are coordinated instead of using a single BS with many antennas. Coherent massive MIMO has the same conclusions, which reinforces the validity of the NC approach.

As part of future work we aim at extending the analysis to a multiuser scenario. We also aim at analyzing the performance difference between selecting the BS with the strongest Rician factor and all the BSs. Last, we aim at providing a framework for the selection of the right BSs to cooperate for a particular user given the parameters of each BS (pathloss, number of antennas, etc.).

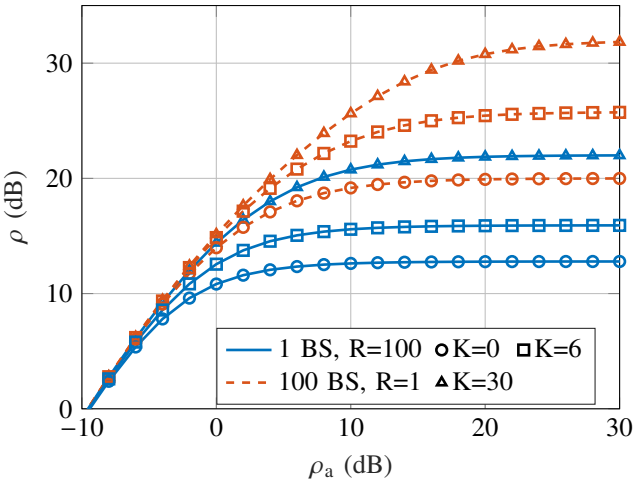

Fig. 8. SINR vs SNR for $M = 64$ and $\delta = 0.5$, for different K.

References

[1] H. Q. Ngo, E. G. Larsson, and T. L. Marzetta, "Energy and spectral efficiency of very large multiuser mimo systems," *IEEE Transactions on Communications*, vol. 61, no. 4, pp. 1436–1449, 2013.

[2] M. J. Lopez-Morales, K. Chen-Hu, and A. Garcia-Armada, "Differential Data-aided Channel Estimation for Up-link Massive SIMO-OFDM," *IEEE Open Journal of the Communications Society*, vol. 1, pp. 976–989, 2020.

[3] M. Chowdhury, A. Manolakos, and A. J. Goldsmith, "Coherent versus noncoherent massive simo systems: Which has better performance?" in *2015 IEEE International Conference on Communications (ICC)*, 2015, pp. 1691–1696.

[4] A. G. Armada and L. Hanzo, "A Non-Coherent Multi-User Large Scale SIMO System Relaying on M-ary DPSK," in *2015 IEEE International Conference on Communications (ICC)*, June 2015, pp. 2517–2522.

[5] L. Sanguinetti, E. Björnson, and J. Hoydis, "Towards massive mimo 2.0: Understanding spatial correlation, interference suppression, and pilot contamination," 2019.

[6] C. He and R. D. Gitlin, "Limiting performance of massive mimo downlink cellular systems," in *2016 Information Theory and Applications Workshop (ITA)*, 2016, pp. 1–6.

[7] V. M. Baeza, A. G. Armada, W. Zhang, M. El-Hajjar, and L. Hanzo, "A Noncoherent Multiuser Large-Scale SIMO System Relying on M-ary DPSK and BICM-ID," *IEEE Transactions on Vehicular Technology*, vol. 67, no. 2, pp. 1809–1814, Feb 2018.

[8] K. Chen-Hu, Y. Liu, and A. Garcia Armada, "Non-Coherent Massive MIMO-OFDM Down-Link based on Differential Modulation," *IEEE Transactions on Vehicular Technology*, pp. 1–1, 2020.

[9] C. Pan, M. Elkashlan, J. Wang, J. Yuan, and L. Hanzo, "User-centric c-ran architecture for ultra-dense 5g networks: Challenges and methodologies," *IEEE Communications Magazine*, vol. 56, no. 6, pp. 14–20, 2018.

[10] J. Zhang, S. Chen, Y. Lin, J. Zheng, B. Ai, and L. Hanzo, "Cell-free massive mimo: A new next-generation paradigm," *IEEE Access*, vol. 7, pp. 99 878–99 888, 2019.

[11] W. Zirwas, "Opportunistic comp for 5g massive mimo multilayer networks," in *WSA 2015; 19th International ITG Workshop on Smart Antennas*, 2015, pp. 1–7.

[12] T. . Chu and L. J. Greenstein, "A semi-empirical representation of antenna diversity gain at cellular and pcs base stations," *IEEE Transactions on Communications*, vol. 45, no. 6, pp. 644–646, 1997.

[13] G. W. Bohrnstedt and A. S. Goldberger, "On the exact covariance of products of random variables," *Journal of the American Statistical Association*, vol. 64, no. 328, pp. 1439–1442, 1969. [Online]. Available: http://www.jstor.org/stable/2286081

[14] R. Gaunt, "Variance-gamma approximation via stein's method," *Electron. J. Probab.*, vol. 19, p. 33 pp., 2014. [Online]. Available: https://doi.org/10.1214/EJP.v19-3020

[15] R. E. Gaunt, "A note on the distribution of the product of zero mean correlated normal random variables," 2018.

[16] R. A. Johnson, D. W. Wichern *et al.*, *Applied multivariate statistical analysis*. Prentice hall Upper Saddle River, NJ, 2002, vol. 5, no. 8.

[17] Y. Feng, M. Wen, J. Zhang, F. Ji, and G. Ning, "Sum of arbitrarily correlated gamma random variables with unequal parameters and its application in wireless communications," in *2016 International Conference on Computing, Networking and Communications (ICNC)*, 2016, pp. 1–5.

[18] L. M. Leemis and J. T. McQueston, "Univariate distribution relationships," *The American Statistician*, vol. 62, no. 1, pp. 45–53, 2008.

[19] Proakis, *Digital Communications 5th Edition*. McGraw Hill, 2007.

[20] A. A. Polegre, F. Riera-Palou, G. Femenias, and A. G. Armada, "Channel hardening in cell-free and user-centric massive mimo networks with spatially correlated ricean fading," *IEEE Access*, vol. 8, pp. 139 827–139 845, 2020.